Occurrence of Vibrational resonance in an oscillator with an asymmetric Toda potential

Olusola Kolebaje [a,c], O. O. Popoola [b], U. E. Vincent [c,d,*]

[a] *Department of Physics, Adeyemi College of Education, 350106, Ondo, Nigeria*
[b] *Department of Physics, University of Ibadan, Ibadan, Nigeria.*
[c] *Department of Physical Sciences, Redeemer's University, P.M.B. 230, Ede, Nigeria.*
[d] *Department of Physics, Lancaster University, Lancaster LA1 4YB, United Kingdom.*

Abstract

Vibrational resonance (VR) is a phenomenon wherein the response of a nonlinear oscillator driven by biharmonic forces with two different frequencies, ω and Ω, such that $\Omega \gg \omega$, is enhanced by optimizing the parameters of high-frequency driving force. In this paper, an counterintuitive scenario in which a biharmonically driven nonlinear oscillator does not vibrate under the well known VR conditions is reported. This behaviour was observed in a system with an integrable and asymmetric Toda potential driven by biharmonic forces in the usual VR configuration. It is shown that with constant dissipation and in the presence of biharmonic forces, VR does not take place, whereas with nonlinear displacement-dependent periodic dissipation multiple VR can be induced at certain values of high-frequency force parameters. Theoretical analysis are validated using numerical computation and Simulink implementation in MATLAB. Finally, the regime in parameter space of the dissipation for optimum occurrence of multiple VR in the Toda oscillator was estimated. This result would be relevant for experimental applications of dual-frequency driven laser models where the Toda potential is extensively employed.

Key words: Oscillations, Vibrations, resonance, Nonlinear dissipation, Toda oscillator

1. Introduction

Since Toda [1,2,3,4] proposed an exponential interaction lattice between particles, now known as the Toda potential more than forty decades ago to explain the phenomenon of self-pulsation, a quasi-periodic pulsation of the output intensity of a solid-state laser in the transient regime, the Toda potential has gained enormous research attention due to its several applications in optics engineering. The major important properties of the Toda potential are its integrability, the existence of periodic and stable solitary wave solutions; as well as exact solutions for the dynamics and the statistical thermodynamics [5,6,7]. The Toda potential is also of special interest because it is the simplest potential function with an Henon type integral or constant of motion and interaction acts only between the neighbouring particles [8]. The aforementioned properties makes the Toda lattice system one of the most prominent subject of research focus, even in the recent times. Indeed, earlier studies employed the Toda potential or lattice for modelling of DNA [9], modelling a linear chain coupled to different heat baths at the ends [10], and the molecular dynamics of muscle contraction [11]. Some new soliton solutions to the Toda lattice were obtained using a modified bilinear Bäcklund transformation [12], Darboux transformation [13,14], exponential-function method [15], hyperbolic function method [16], and extended tanh-function approach, with the asymptotic stability proved in [17]. The Toda lattice has been shown to be super-integrable because for every N degrees of freedom, it possesses $2N-1$ independent constants of motion [7]. In addition, numerical solution for the Toda lattice has been obtained via the Variational Iteration Method [18], and Adomian Decomposition Method [19].

More pertinent to the present study, Toda lattice has been successfully used to model different classes of lasers such as a damped an-harmonic oscillator subject to the Toda potential (Otto and Politi [20]), modulated lasers [21,22], class-B lasers [23,24] and bad-cavity lasers [25,26]. Cialdi *et al.* [24] confirmed experimentally that the Toda oscillator model describes excellently the early stage dynam-

* corresponding author.
Email address: u.vincent@lancaster.ac.uk (U. E. Vincent).

ics of the Nd:YAG laser. Investigations on the dynamics of the Toda oscillator has revealed several intriguing dynamical behaviours including sub- or supercritical Andronov-Hopf bifurcation born from stable or unstable branch of periodic solutions, period doubling, saddle-node, Neimark-Saker bifurcations, fold-bifurcations, chaos and hyperchaos in coupled antiphase driven Toda oscillators [27,28,29,30]. In all the previous studies, the Toda oscillators were driven mostly by a single sinusoidal force. In the paper by Kim *et al.* [31], intermittent route to strange nonchaotic attractors was reported in a dual-frequency driven Toda oscillator at two incommensurate frequencies. However, to the best of our knowledge there is no report on the occurrence of vibrational resonance (VR) [32] in dual-frequency driven Toda oscillator.

Motivated by the foregoing, we investigate the phenomenon of vibrational resonance (VR), first studied by Landa and McClintock [32] - manifesting in nonlinear systems driven by a biharmonic external force with two different frequencies ω and Ω; a low-frequency force $F\cos\omega t$ and a high-frequency force $G\cos\Omega t$ [33]. The amplification of the weak input signal by the biharmonic periodic external force carries significant importance in communications [34,35], laser physics [36], acoustics [37], medicine [38], neuroscience [39], geosciences [40], and ecology [41]. Following the work of Landa and McClintock [32], Gitterman [42] and Blekhman and Landa [43] developed theoretical techniques for analysing VR. Consequently, the occurrence of VR has been investigated theoretically and numerically in monostable systems [44,45,46], multistable systems [44], excitable systems [47], and time-delayed systems [48], asymmetric Duffing oscillator [46,49], biological nonlinear maps [50], the quintic oscillator [44,45], a bistable system [51], gene transcriptional regulatory system [52,53]; and more recently in the FitzHugh-Nagumo model driven by a bichromatic excitation [54], nonlinearly-damped oscillators [55,56,57], asymmetrical deformable oscillator [58], in time-delay gene transcriptional regulatory system [59] and in systems with rough potentials [60], to mention but a few. The majority of the above-mentioned results demonstrated the effects and roles of the high-frequency force parameters G and Ω on the occurrence of VR. Recently, the effect of depth and location of the potential well on VR was reported in a quintic oscillator [61]. Furthermore, nonlinearity in the damping coefficient plays significant contributory roles in the occurrence of VR [55,56,57]. Very recently, a new body of research in connection with the VR phenomenon in the quantum domain has emerged [62,63]. In addition, a recent review presented a new formalism for describing VR in position-dependent mass systems [64]. The wide incidence of VR observed in many kinds of system are linked to its potential applications in, for instance, detection of weak random signals [65], improving weak aperiodic signals [66], amplification of an auto-dyne signals in vertical-cavity surface-emitting laser [67], enhancing weak signal with arbitrary high-frequencies [68,69], detection of weak signals in the presence of strong background noise [70].

In this paper, we report the result of an analysis on possible occurrence of VR in an oscillator with an integrable and asymmetric Toda potential. We will show, counter-intuitively, that under the actions of dual-frequency signal forces, the Toda oscillator with constant dissipation coefficient does not vibrate. However, with periodic dissipation in place, VR is induced. We employed both analytical and numerical treatments to investigate the mechanism of the VR and provide clear evidence that introducing periodicity into the otherwise constant damping coefficient can induce VR in the presence of the dual-frequency driving force. The present result differs significantly from previous reports in which nonlinear dissipation enhances vibration-induced resonances as reported in [55,56,57]. The paper is organized as follows: the model is introduced in Section 2. The theoretical and numerical analysis of VR are presented in Section 3 and 4 respectively with the discussions and conclusion provided in Section 5.

2. The model

The model is a generalized damped and bi-harmonically driven nonlinear system with a Toda potential. The equation of motion is given by [31]

$$\frac{d^2x}{dt^2} + \nu(x)\frac{dx}{dt} + \frac{dU}{dx} = F\cos\omega t + G\cos\Omega t, \tag{1}$$

where $F\cos\omega t$ is the low-frequency force with frequency ω while $G\cos\Omega t$ is the high-frequency force with frequency Ω; and $\Omega >> \omega$. In Eq. (1), we have included a 2π-periodic multiplicative displacement-dependent damping term, $\nu(x)$ which is a function of k_0 and ϵ denoting, respectively the damping amplitude and the strength of the dissipation in the form

$$\nu(x) = k_0\left(1 + \epsilon\cos x\right); \tag{2}$$

while $U(x)$ is the well known Toda potential given by

$$U(x) = e^x - x + 1. \tag{3}$$

The Toda potential has an extremely asymmetric curvature and a linear dependence on the displacement x in the $x < 0$ region when $\lim_{x\to-\infty} U(x) = -x + 1$, which is equivalent to free fall dynamic. In the region $x > 0$, i.e. when $\lim_{x\to\infty} U(x) = e^x$ the system contains a very hard spring. In the analysis that will follow, we will show that the displacement-dependent periodic damping is essential for the occurrence of VR and that in its absence, the Toda oscillator will not vibrate even in the presence of dual-frequency forcing. Using Eq. (2) and Eq. (3) in Eq. (1), the system to be analysed becomes

$$\ddot{x} + k_0\left(1 + \epsilon\cos x\right)\dot{x} + e^x - 1 = F\cos\omega t + G\cos\Omega t. \tag{4}$$

When $\epsilon = 0$, system (2) reduces to the exact model of a quasiperiodically forced Toda oscillator exhibiting non-trivial intermittent route to strange nonchaotic attractors

(SNAs) reported in [31]. Furthermore, if only one external driving force is considered for constant damping, i.e. $\epsilon = 0$, system (2) reduces to the well investigated driven Toda oscillator exhibiting abundant varieties of bifurcation structures including period-doubling, devil's staircase and chaos [27]. This system possesses unique asymmetry that is at variance with oscillators in Duffing family. In fact, its arguably, a good prototypical and simplest model for asymmetric oscillators; and as such has been used to model a nonlinear RLC circuit [71]. Figures 1 and 2 illustrate the salient features of the Toda potential and the periodic damping in Eq. (4). The amplitude and location of local minima and maxima of the periodic damping depends on the sign of the damping amplitude k_0 and strength of inhomogeneity ϵ.

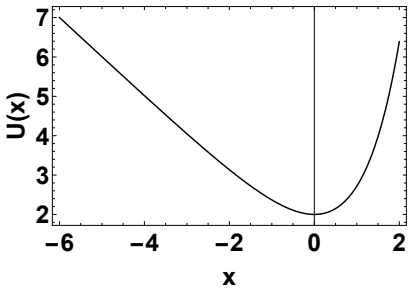

Fig. 1. Shape of the Toda Potential $U(x) = e^x - x + 1$.

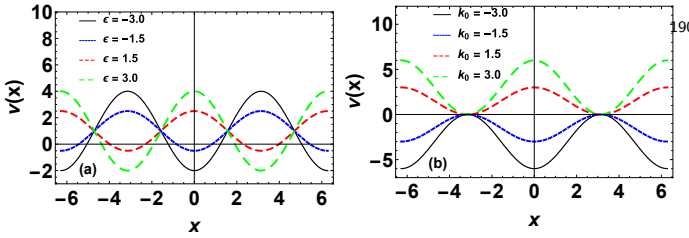

Fig. 2. Shape of the Periodic Damping Term $\nu(x)$ for; (a) four values of ϵ with $k_0 = 1$ (b) four values of k_0 with $\epsilon = 1$.

3. Theoretical Analysis

To examine VR theoretically, we employ the method of separation of motion to separate Eq. (4) into slow and fast motion. Since $\Omega \gg \omega$, we can assume that the solution of Eq. (4) is of the form $x(t) = X(t) + \psi(t, \tau = \Omega t)$, where X and ψ are the slow motion with frequency ω and period $2\pi/\omega$ and fast motion in fast time τ with frequency Ω and period $2\pi/\Omega$, respectively. The mean value of ψ with respect to time τ is given by

$$\langle\psi\rangle = \frac{1}{2\pi}\int_0^{2\pi} \psi(\tau)d\tau = 0. \tag{5}$$

Substituting $x = X + \psi$ and Eq. (5) into Eq. (4), we obtain

$$\ddot{X} + \ddot{\psi} + k_0\left[1 + \epsilon\cos X\cos\psi - \epsilon\sin X\sin\psi\right](\dot{X} + \dot{\psi}) + e^{X+\psi} - 1 = F\cos\omega t + G\cos\Omega t. \tag{6}$$

Since ψ is a periodic function in fast time τ, then by averaging both sides of Eq. (6) over the period $\left[0, \frac{2\pi}{\Omega}\right]$, then the equation for the slow motion can be obtained as

$$\ddot{X} + k_0\left[1 + \epsilon\cos X\langle\cos\psi\rangle - \epsilon\sin X\langle\sin\psi\rangle\right]\dot{X} + e^X\langle e^\psi\rangle - 1 = F\cos$$

The equation for the fast motion ψ is obtained by subtracting Eq. (7) from Eq. (6) and by inertial approximation $\ddot{\psi} >> \dot{\psi} >> \psi$, it reduces to $\ddot{\psi} = G\cos\Omega t$, which has the solution

$$\psi(\tau) = -\frac{G}{\Omega^2}\cos\tau. \tag{8}$$

With ψ in Eq. (8), we obtain the mean values

$$\begin{aligned}\langle\sin\psi\rangle &= \frac{1}{2\pi}\int_0^{2\pi}\sin\psi(\tau)d\tau = 0,\\ \langle\cos\psi\rangle &= \frac{1}{2\pi}\int_0^{2\pi}\cos\psi(\tau)d\tau = J_0\left(G/\Omega^2\right),\\ \langle e^\psi\rangle &= \frac{1}{2\pi}\int_0^{2\pi}e^{\psi(\tau)}d\tau = I_0\left(G/\Omega^2\right),\end{aligned} \tag{9}$$

where $J_0\left(G/\Omega^2\right)$ and $I_0\left(G/\Omega^2\right)$ are respectively the zeroth-order Bessel function of the first kind and the zeroth-order modified Bessel function of the first kind. Eq. (9) allows us to simplify Eq. (7), so that the equation for the slow motion becomes

$$\ddot{X} + k_0\left[1 + \epsilon J_0\left(G/\Omega^2\right)\cos X\right]\dot{X} + I_0\left(G/\Omega^2\right)e^X - 1 = F\cos\omega t.(1$$

Eq. (10) can be re-written as the equation of motion of a system in the form

$$\ddot{X} + \lambda_{eff}\dot{X} + \frac{dV_{eff}(X)}{dX} = F\cos\omega t \tag{11}$$

where

$$V_{eff} = I_0\left(G/\Omega^2\right)e^X - X \tag{12}$$

and

$$\lambda_{eff} = k_0\left[1 + \epsilon J_0\left(G/\Omega^2\right)\cos X\right] \tag{13}$$

are the effective potential and effective damping coefficient respectively. The shape and number of local minima and maxima of the effective potential depends on the parameters G, Ω and β. Figure 3 shows that the location of local minima changes with increasing G and Ω respectively.

The effective potential of the system is always a single well with a minimum located at

$$X^* = -\ln\left(I_0\left(\frac{G}{\Omega^2}\right)\right) \tag{14}$$

The equation of motion for the deviation variable $Y = X - X^*$ is given by

$$\ddot{Y} + k_0\left[1 + \epsilon J_0\cos Y + X^*\right]\dot{Y} + I_0 e^{X^*}e^Y - 1 = F\cos\omega t.(15)$$

$$\ddot{Y} + k_0\left[1 + \epsilon J_0\cos X^*\cos Y - \epsilon J_0\sin X^*\sin Y\right]\dot{Y} + e^Y - 1 = F\cos$$

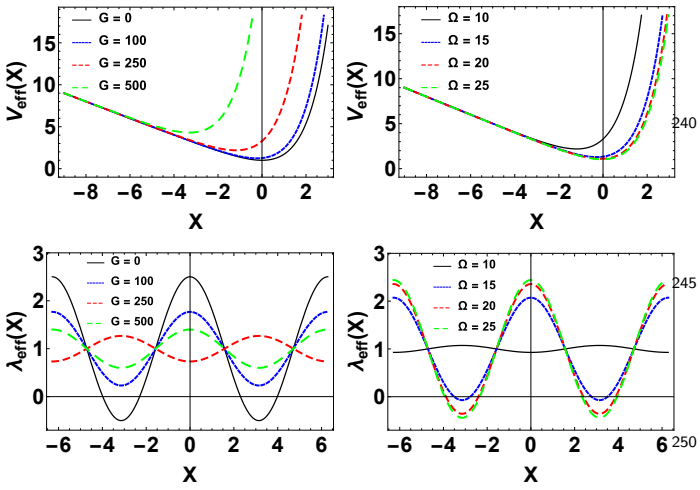

Fig. 3. The effective potential $V_{eff}(X)$ for (a) four values of G with $\Omega = 10$ (b) four values of Ω with $G = 250$ and the effective damping $\lambda_{eff}(X)$ with $k_0 = 1$, $\epsilon = 1.5$ for (c) four values of G with $\Omega = 10$ (d) four values of Ω with $G = 250$.

For $F << 1$, then $|Y| << 1$ and we can approximate $\cos Y \approx 1$, $\sin Y \approx Y$ and $e^Y \approx 1 + Y$, so Eq. (16) becomes

$$\ddot{Y} + k_0 \left[1 + \epsilon J_0 \cos X^* - \epsilon J_0 \sin X^* Y\right] \dot{Y} + Y = F \cos \omega t. \quad (17)$$

By neglecting the nonlinear terms in Eq. 17, we obtain an approximate damped and periodically forced linear equation of the form

$$\ddot{Y} + \lambda \dot{Y} + Y = F \cos \omega t, \quad (18)$$

where

$$\lambda = k_0 \left[1 + \epsilon J_0 \left(\frac{G}{\Omega^2}\right) \cos \alpha\right] \quad (19)$$

and $\alpha = \ln \left[I_0 \left(\frac{G}{\Omega^2}\right)^{-1}\right]$. The solution of Eq. (18) in the long-time limit ($t \to \infty$) is $Y(t) = A_L \cos(\omega t + \phi)$; where $A_L = F/\sqrt{S}$ and

$$S = (1 - \omega^2)^2 + \lambda^2 \omega^2, \qquad \phi = \tan^{-1}\left[\frac{\lambda \omega}{\omega^2 - 1}\right]. \quad (20)$$

Hence, the response amplitude, which is the measure of amplification of the input signal by the high frequency signal is defined by

$$Q = \frac{A_L}{F} = \frac{1}{\sqrt{(1 - \omega^2)^2 + \lambda^2 \omega^2}}. \quad (21)$$

Notably, for constant dissipation or damping, i.e. $\epsilon = 0$, λ in Eq. (19) reduces to $\lambda = k_0$. Consequently, theoretical analysis based on the method of separation of motion suggests that, the Toda oscillator (1) does not admit VR for constant dissipation or damping on account that the response amplitude Q in Eq. (21) is independent on the parameters G and Ω of the high-frequency force. Remarkably, a variation in the response amplitude with the high-frequency force parameters G and Ω may appear in the numerical investigations. Whether the observed variation is sufficiently significant to be regarded as an amplification or de-amplification of the input signal is an open issue for further investigation. However, when ϵ takes on nonzero values multiple VR can occur in different ϵ-regimes - which is the main result of this paper as we shall further illustrate. It is emphasized here that the non-occurrence of VR for constant dissipation is remarkably counterintuitive and at variant with results obtained from the Duffing oscillator family as well as all the previous results obtained other systems.

Now, let us analyze the occurrence of vibrational resonance as G is varied. From Eq. (20), we see that $S_G = 2\lambda\omega^2\lambda_G$, where $\lambda_G = d\lambda/dG$. Hence, VR is attained when $S_G = 0$, which could be achieved subject to the following conditions: (i) $\lambda = 0$ or (ii) $\lambda_G = 0$ with $\lambda_{GG} = d^2\lambda/dG^2|_{G_{VR}} > 0$.

Since $k_0 \neq 0$, then $\lambda = 0$ when

$$\frac{1}{\epsilon} = -J_0 \left(\frac{G}{\Omega^2}\right) \cos \alpha \quad (22)$$

and the resonance value is given by $Q_{\lambda=0} = 1/|1 - \omega^2|$, $\omega^2 \neq 1$; which satisfies case (i). Hence, for fixed values of the other system parameters, the response amplitude $Q_{\lambda=0}$ is achieved at values of G that satisfy Eq. (22). Figure 4 shows the values of G for which $\lambda = 0$ for selected values of Ω and ϵ. Figure 4 shows that $\lambda = 0$ only for ϵ values in the region $-1 < \epsilon^{-1} < \epsilon_0^{-1}$ with multiple VR due to $\lambda = 0$ occuring only for ϵ values in the region $\epsilon_1^{-1} < \epsilon^{-1} < \epsilon_0^{-1}$, where $\epsilon_1^{-1} = -0.3243$ and $\epsilon_0^{-1} = 0.0935$. Also, the range of values of G for which $\lambda = 0$ increases as Ω decreases. That is, resonance due to $\lambda = 0$ occurs only for $\epsilon < -1$ and $\epsilon > \epsilon_0$. Hence, for $-1 < \epsilon < \epsilon_0$, VR will not occur since $\lambda = 0$.

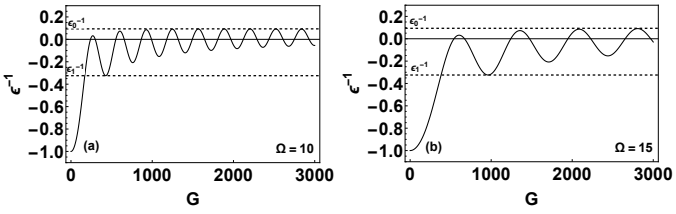

Fig. 4. The Plot of $1/\epsilon$ against G from Eq. (22) with (a) $\Omega = 10$ and (b) $\Omega = 15$

The second condition, i.e. $\lambda_G = 0$ is such that

$$\lambda_G = \frac{k_0 \epsilon}{\Omega^2} \left[-J_1 \cos \alpha + \frac{I_1 J_0}{I_0} \sin \alpha\right] \quad (23)$$

where J_1 and I_1 are respectively the Bessel function of the first kind of order 1 and the modified Bessel function of the first kind of order one. From Eq. (23), since $k_0 \neq 0$, for $\lambda_G = 0$ and $\lambda_{GG} > 0$, then there are peaks in the response amplitude for G that satisfy

$$J_1 \cos \alpha = \frac{I_1 J_0}{I_0} \sin \alpha. \quad (24)$$

The roots of Eq. (24), G_{VR}, occur at the critical points of λ. For $k_0 > 0$, G_{VR} occur at the values of G for which λ

is at a local minimum. In addition, for $k_0 < 0$, G_{VR} values at which VR occurs coincide with the local maxima of λ. The minima and maxima values of λ are located at G_{VR} that satisfy (24). It was observed that the oscillatory nature of the effective damping term λ gives rise to oscillatory variation of the response amplitude Q with VR taking place at the minima or maxima of λ for $k_0 > 0$ and $k_0 < 0$ respectively. Thus, one can infer that the choice of damping nature would determine the nature of the response curve.

We remark that not all values of G_{VR} due to $\lambda_G = 0$ corresponds to VR, since the peak produced in the Q-curve does not necessarily imply a gain in the response amplitude at $G = 0$. The Q value at G_{VR} due to $\lambda_G = 0$ corresponds to VR when $Q_{G_{VR}} > Q_{G=0}$ with

$$Q_{G=0} = \frac{1}{\sqrt{(1-\omega^2)^2 + \lambda_{G=0}^2 \omega^2}}, \qquad \lambda_{G=0} = k_0(1+\epsilon). \quad (25)$$

The G values for which $\lambda_{G=0}$ produces a gain in the response amplitude at $Q_{G=0}$ is subject to the condition that: $|\lambda_{G_{VR}}| < |\lambda_{G=0}|$ is satisfied.

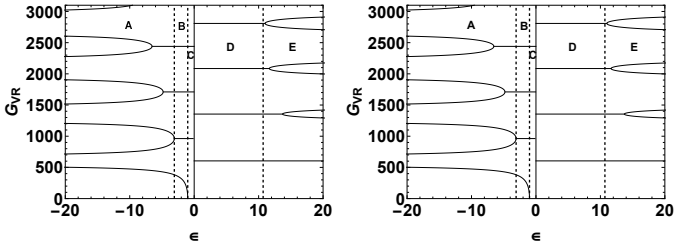

Fig. 5. Variation of the theoretically predicted G_{VR} with the parameter ϵ for (a) $\Omega = 10$ (b) $\Omega = 15$. The vertical dashed lines are at $\epsilon = \epsilon_1 = -3.08$, $\epsilon = -1$ and $\epsilon = \epsilon_0 = 10.70$.

In Figure 5, we plot the theoretically calculated G_{VR} against the strength of inhomogeneity of the system ϵ for $\Omega = 10$ and $\Omega = 15$ respectively. The shape of the response curves can be predicted and understood from Figure 5 by analysing the Regions A-E of ϵ values.

(i) Region A ($\epsilon < \epsilon_1$): Multiple VR occurs because both conditions $\lambda_G = 0$ and $\lambda = 0$ are satisfied.

(ii) Region B ($\epsilon_1 < \epsilon < -1$): VR occur only at one value of G when $\lambda = 0$ and at certain values of G when $\lambda_G = 0$, provided $|\lambda_{G_{VR}}| < |\lambda_{G=0}|$.

(iii) Region C ($-1 < \epsilon < 0$): No occurrence of VR.

(iv) Region D ($0 < \epsilon < \epsilon_0$): Multiple VR occurs because only the condition $\lambda_G = 0$ is satisfied.

(v) Region E ($\epsilon > \epsilon_0$): Multiple VR occurs because both conditions $\lambda_G = 0$ and $\lambda = 0$ are satisfied.

In general, for $-1 < \epsilon < \epsilon_0$, multiple VR due to $\lambda_G = 0$ only occurs for $\epsilon > 0$ but there is no resonance for $\epsilon < 0$. However, for $\epsilon < \epsilon_1$ or $\epsilon > \epsilon_0$, VR peaks due to $\lambda_G = 0$ and $\lambda = 0$ are observed. In Figures 6 and 8, the theoretically computed response amplitude Q against G is plotted for different ϵ values corresponding to the Regions A-E for $\Omega = 10$ and $\Omega = 15$ respectively. To achieve optimal VR phenomena in the Toda oscillator model, periodic dissipation with strength of inhomogeneity ϵ values in regions A, D and E earlier outlined is presented. Furthermore, the number of G_{VR} points decreases with increase in the high-signal frequency Ω.

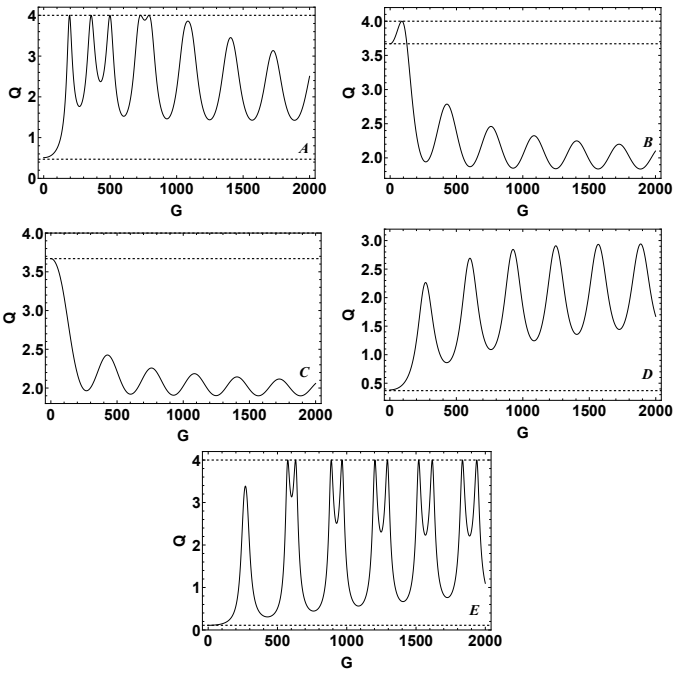

Fig. 6. Plot of theoretically computed response amplitude Q as a function of G for $\omega^2 = 0.75$, $k_0 = 0.5$, $\Omega = 10$ and ϵ values in Regions A-E.

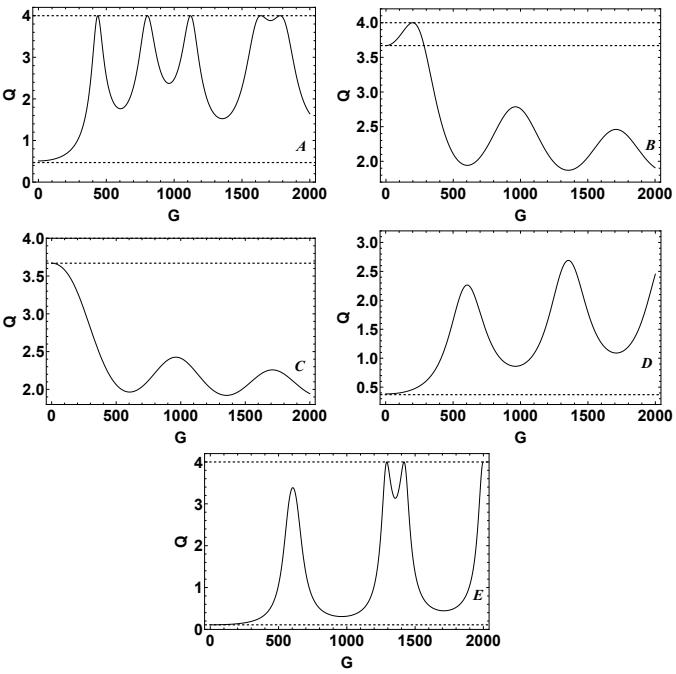

Fig. 7. Plot of theoretically computed response amplitude Q as a function of G for $\omega^2 = 0.75$, $k_0 = 0.5$, $\Omega = 15$ and ϵ values in Regions A-E.

4. Numerical and Simulink Verification

The second-order nonautonomous ordinary differential equation (ODE) given by Eq. (4) can be re-expressed as an equivalent system of two first-order autonomous ODEs of the form:

$$\frac{dx}{dt} = y;$$
$$\frac{dy}{dt} = -k_0\left(1+\epsilon\cos x\right)y - e^x + 1 + F\cos\omega t + G\cos\Omega t \quad (26)$$

Numerical integration of Eq. (26) is achieved via the fourth-order Runge-Kutta scheme with a suitable step size over the time interval nT with $T = 2\pi/\omega$ being the period of the low-frequency force F and n the number of complete oscillations.

Following the numerical integration of Eq. (26), the response amplitude Q can then be calculated numerically using the components of the Fourier spectrum of the time series of x given by

$$Q = \frac{A}{F} = \frac{\sqrt{Q_S^2 + Q_C^2}}{F} \quad (27)$$

where

$$Q_S = \frac{2}{nT}\int_0^{nT} x(t)\sin\omega t dt, \qquad Q_C = \frac{2}{nT}\int_0^{nT} x(t)\cos\omega t dt. \quad (28)$$

n can be taken to be a suitably large value, say, 200.

We first examine and compare theoretically and numerically obtained dependence of the response amplitude Q on the damping amplitude k_0 and strength of inhomogeneity ϵ. In Figure 8, we have presented plot of the response amplitude Q as a function of the high-frequency force G, for various values of the strength of inhomogeneity ϵ at a fixed k_0 value; while in Figure 9, we present plot of the response amplitude Q as a function of the high-frequency force G, for various values of the damping amplitude k_0 at a fixed ϵ value. The response amplitude Q calculated from theory and numerics are represented by the continuous curve and marker points respectively. In Figure 8, different ϵ values were chosen, i.e. $\epsilon = -2.5, 1.5$ and 11.5 in different parameter regimes, namely, negative, low and high values of the damping inhomogeneity ϵ. Figures 8 and 9 shows that there is good agreement between the theoretically and numerically obtained response Q. Moreover, the shape and trend of the theory (continuous curve) and numerics (solid marker points) are in good agreement. An increase in the value of Ω leads to a decrease in the frequency of occurrence of the resonance points. With the variation in the damping amplitude k_0 at a fixed value of ϵ, the high-frequency force G values at which VR occurs remains unchanged. However, the position of the maxima and minima of the response amplitude Q increases with decrease in the damping amplitude.

We implemented the Toda oscillator model given by Eq. (26) in MATLAB-Simulink. Simulink is a MATLAB-based environment for modelling and simulating dynamical systems. A block diagram of the system of equations was created in MATLAB-Simulink and is shown in Figure 10. *Subsystem 1* in Figure 10 has *input 1* and *input 2* as x and 1 respectively and an output that performs $k_0(1+\epsilon\cos x)$. *Subsystem 2* is a time-input block with two outputs: *output 1* and *output 2* which represents the driving functions, $F\cos\omega t$ and $G\cos\Omega t$, respectively. The data obtained from the Simulink environment was plotted in MATLAB and are presented in Figures 11 and 12. Figures 11 and 12 show that the Simulink implementation of the Toda oscillator model given by Eq. (26) was in excellent agreement with the theoretically calculated response amplitude Q given by Eq. (21).

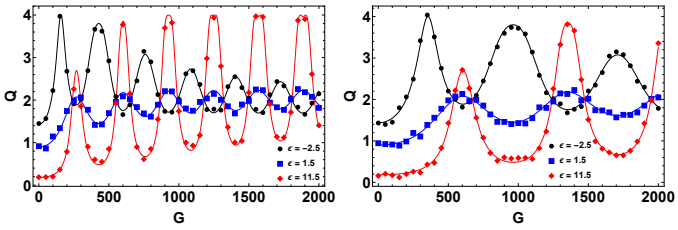

Fig. 8. Dependence of the response amplitude Q on G for three values of the damping amplitude $\epsilon = -2.5$, $\epsilon = 1.5$ and $\epsilon = 11.5$ with the other parameters fixed at $F = 0.2$, $\omega^2 = 0.75$, $k_0 = 0.5$, $\Omega = 10$ (left-panel) and $\Omega = 15$ (right-panel). The continuous curve and solid markers represent the theoretically and numerically computed values of Q respectively.

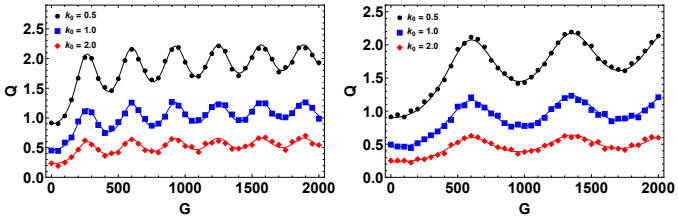

Fig. 9. Dependence of the response amplitude Q on G for three values of the damping amplitude $k_0 = 0.5$, $k_0 = 1.0$ and $k_0 = 2.0$ with the other parameters fixed at $F = 0.2$, $\omega^2 = 0.75$, $\epsilon = 1.5$, $\Omega = 10$ (left-panel) and $\Omega = 15$ (right-panel). The continuous curve and solid markers represent the theoretically and numerically computed values of Q respectively.

5. Conclusion

In this paper, we have theoretically studied and numerically verified the occurrence of the phenomenon of vibrational resonance in a damped and bi-harmonically driven Toda oscillator model with asymmetric potential. Theoretical analysis of VR was carried out by first separating the model into fast and slow motions. The response amplitude was then obtained from the linearised equation of the slow motion. One of the most striking and remarkable observations was the non-occurrence of VR when the damping coefficient take on constant values. However with displacement-dependent periodic damping, multiple resonances are induced for a wide range of the damping parameters. The

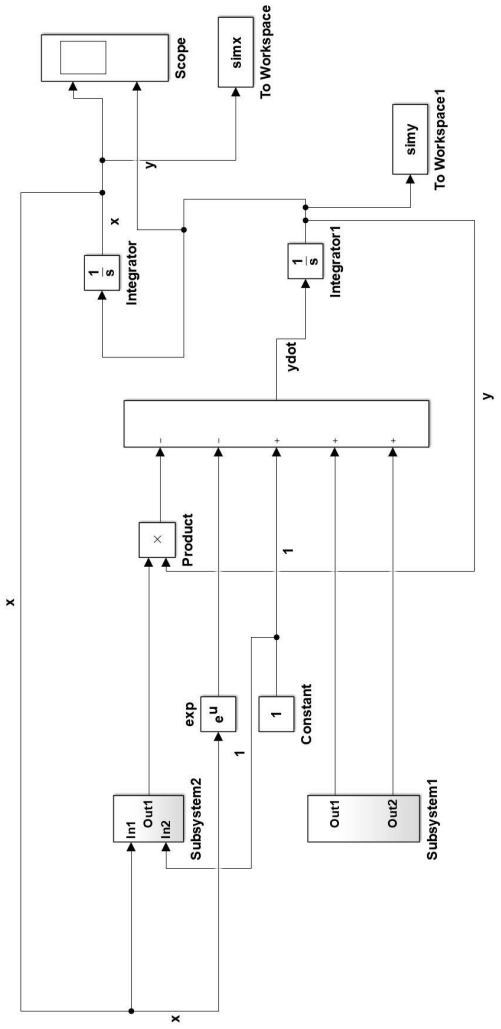

Fig. 10. Simulink implementation of the Toda oscillator system 1.

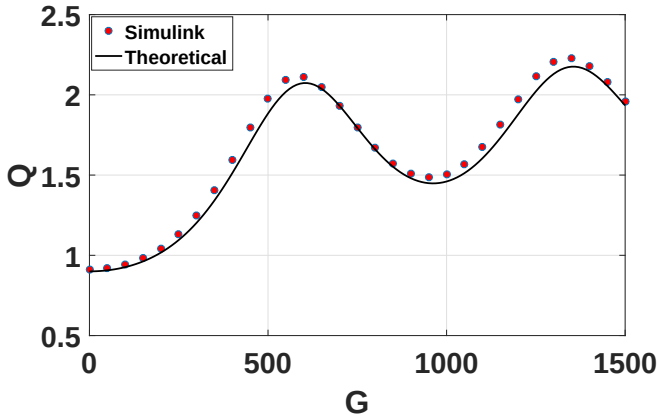

Fig. 11. The response amplitude Q as a function of G computed theoretically (continuous line) and Simulink simulation (red dots) of the Toda system Eq. (26) for $\epsilon = 1.5$, $F = 0.2$, $\omega^2 = 0.75$, $k_0 = 0.5$ and $\Omega = 15$.

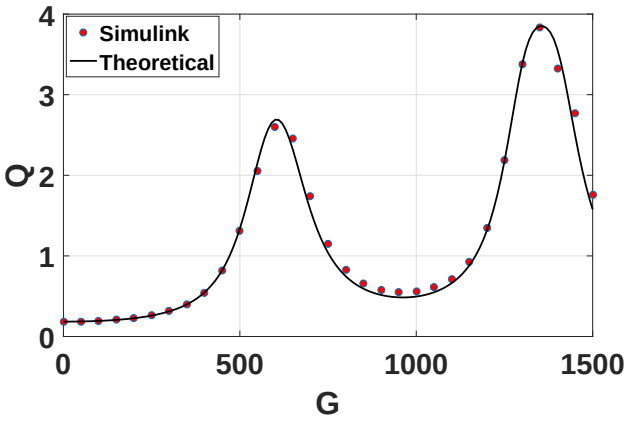

Fig. 12. The response amplitude Q as a function of G computed theoretically (continuous line) and Simulink simulation (red dots) of the Toda system Eq. (26) for $\epsilon = 11.5$, $F = 0.2$, $\omega^2 = 0.75$, $k_0 = 0.5$ and $\Omega = 15$.

strength of displacement-dependent periodic dissipation ϵ impacts significantly on the nature and occurrence of VR. We emphasize that the present result is a departure from previous reports in which nonlinear dissipation enhances vibration-induced resonances as reported in [55,56,57]. The study showed that multiple VR is admissible in the model with the Toda potential for ϵ values in the region $\epsilon < -1.5$ and $\epsilon > 0$ with the highest number of VR points observed for $\epsilon > \epsilon_0$, where ϵ_0 is a threshold that depends on the high-frequency Ω values. Numerical approach was also employed to confirm the theoretical analysis and very good agreement was achieved. This study provided insight into the conditions and the system parameter (k_0 and ϵ) regime for which one can achieve VR in the Toda oscillator model. The results have great potential for modelling modulated lasers [21,22], class-B lasers [23,24] and bad-cavity lasers [25] for laser output amplification. In this regard, we implemented the dual-frequency driven Toda oscillator model using MATLAB-Simulink, compared the response output from the MATLAB-Simulink with theoretical results, and found excellent agreement. Finally, we remark that the effects of dual-frequency driving presented here can be implemented in the context of the experimental configuration of class-B lasers presented by Cialdi et al. [24].

6. Acknowledgments

We acknowledge useful discussions with Dr. B. R. Nana-Nbendjo. The authors thank the anonymous Reviewers for their invaluable comments and suggestions that improved the quality and depth of this paper.

References

[1] M. Toda, Waves in nonlinear lattice, Progress of Theoretical Physics Supplement 45 (1970) 174–200.
[2] M. Toda, Studies of a non-linear lattice, Physics Reports 18 (1) (1975) 1 – 123.
[3] M. Toda, Theory of Nonlinear Waves and Solitons, Kluwer, Dordrecht, 1989.

[4] G. Teschl, Almost everything you always wanted to know about the Toda Equation, Jahresber. Deutsch. Math.-Verein. 103 (4) (2001) 149–162.

[5] W. Ebeling, U. Erdmann, J. Dunkel, M. Jenssen, Nonlinear dynamics and fluctuations of dissipative Toda chains, Journal of Statistical Physics 101 (1) (2000) 443–457.

[6] V. N. Likhachev, T. Y. Astakhova, G. A. Vinogradov, Thermodynamics and ergodicity of finite one-dimensional Toda and Morse lattices, Physics Letters A 354 (4) (2006) 264 – 270.

[7] M. A. Agrotis, P. A. Damianou, C. Sophocleous, The Toda lattice is super-integrable, Physica A 365 (1) (2006) 235 – 243.

[8] M. Hénon, Integrals of the Toda lattice, Phys. Rev. B 9 (1974) 1921–1923.

[9] V. Muto, A. C. Scott, P. L. Christiansen, Thermally generated solitons in a Toda lattice model of DNA, Physics Letters A 136 (1-2) (1989) 33 – 36.

[10] F. Mokross, H. Buttner, Thermally generated solitons in a Toda lattice model of DNA, J. Phys. C: Solid State Phys. 16 (23) (1983) 4539.

[11] S. Yomosa, Toda-lattice solitons in α-helical proteins, J. Phys. Soc. Jpn. 53 (10) (1984) 3692–3698.

[12] M. Sun, S. Deng, D. Chen, The backlund transformation and novel solutions for the Toda lattice, Chaos, Solitons & Fractals 23 (4) (2005) 1169 – 1175.

[13] X. Wen, N-fold Darboux Transformation and soliton solutions for Toda lattice equation, Reports on Mathematical Physics 68 (2) (2011) 211 – 223.

[14] X. Xu, H. Yang, Y. Sun, Darboux transformation of the modified Toda lattice equation, Mod. Phys. Lett. B 20 (11) (2006) 641.

[15] C. Dai, Y. Wang, Exact travelling wave solutions of Toda lattice equations obtained via the exp-function method, Zeitschrift für Naturforschung A 63 (10-11) (2014) 657 – 662.

[16] Z. Jia-Min, Hyperbolic function method for solving nonlinear differential-different equations, Chinese Physics 14 (7) (2005) 1290.

[17] T. Mizumachi, P. R.L., Asymptotic stability of Toda lattice solitons, Nonlinearity 21 (9) (2008) 2099.

[18] R. Mokhtari, Variational iteration method for solving nonlinear differential- difference equations, International Journal of Nonlinear Sciences and Numerical Simulation 9 (1) (2011) 19 – 24.

[19] L. Wu, L. Xie, J. Zhang, Adomian decomposition method for nonlinear differential-difference equations, Communications in Nonlinear Science and Numerical Simulation 14 (1) (2009) 12 – 18.

[20] G. L. Oppo, A. Politi, Toda potential in laser equations, Zeitschrift für Physik B - Condensed Matter 59 (1985) 111–115.

[21] P. A. Braza, Phase jumps of π in a laser with a periodically modulated injected signal, Physica D 134 (4) (1999) 394 – 405.

[22] Y. Khanin, Fundamentals of Laser Dynamics, Cambridge, 2006.

[23] Y. Lien, S. de Vries, M. van Exter, J. Woerdman, Lasers as Toda oscillators, J. Opt. Soc. Am. B 19 (6) (2002) 1461–1466.

[24] S. Cialdi, F. Castelli, F. Prati, Lasers as Toda oscillators: An experimental confirmation, Optics Communications 287 (2013) 176 – 179.

[25] T. Ogawa, Stochastic Toda-oscillator model of the bad-cavity laser, Phys. Rev. A 42 (1990) 4210–4225.

[26] T. Ogawa, Quasiperiodic instability and chaos in the bad-cavity laser with modulated inversion: Numerical analysis of a Toda oscillator system, Phys. Rev. A 37 (1988) 4286–4302.

[27] T. Kurz, W. Lauterborn, Bifurcation structure of the Toda oscillator, Physical Review A 37 (3) (1988) 1029–1031.

[28] B. K. Goswami, Observation of some new phenomena involving period tripling and period doubling, International Journal of Bifurcation and Chaos 05 (01) (1995) 303–312.

[29] A. Dvorak, P. Kuzma, P. Perlikowski, V. Astakhov, T. Kapitaniak, Dynamics of three Toda oscillators with nonlinear unidirectional coupling, The European Physical Journal Special Topics 222 (10) (2013) 2429–2439.

[30] N. V. Stankevich, A. Dvorak, V. Astakhov, P. Jaros, M. Kapitaniak, P. Perlikowski, T. Kapitaniak, Chaos and hyperchaos in coupled antiphase driven Toda oscillators, Regular and Chaotic Dynamics 23 (1) (2018) 120–126.

[31] S.-Y. Kim, W. Lim, Universal mechanism for the intermittent route to strange nonchaotic attractors in quasiperiodically forced systems, J. Phys. A: Math & Gen 37 (25) (2004) 6477–6489.

[32] P. S. Landa, P. V. E. McClintock, Vibrational resonance, J. Phys. A: Math. Gen. 33 (2000) 433–438.

[33] S. Rajasekar, M. A. F. Sanjuan, Nonlinear Resonances, Springer Series in Synergetics, Springer, Switzerland, 2016.

[34] H. C. Gerhardt, Significance of two frequency bands in long distance vocal communications in the green tree frog, Nature 261 (1976) 692–694.

[35] G. P. Agrawal, Fiber-Optic Communication Systems, Wiley, New York, 1992.

[36] D. C. Su, M. H. Chiu, C. D. Chen, Simple two-frequency laser, Precis. Eng. 18 (2-3) (1996) 161–163.

[37] A. O. Maksimov, On the subharmonic emission of gas bubbles under two-frequency excitation, Ultrasonics 35 (1997) 79–86.

[38] K. Harikrishnan, G. Ambika, Resonance phenomena in discrete systems with bichromatic input signal, EuroPhys. J. B 61 (3) (2008) 343–353.

[39] D. M. Ackermann, N. Bhadra, E. L. Foldes, K. L. Kilgore, Conduction block of whole nerve without onset firing using combined high frequency and direct current, Med. Biol. Eng. Comput. 49 (2) (2011) 241–251.

[40] C. Jeevarathinam, S. Rajasekar, M. A. F. Sanjuan, Vibrational resonance in groundwater-dependent plant ecosystems, Ecol. Complex. 15 (2013) 33–42.

[41] L. Ridolfi, P. D'Odorico, F. Laio, Vegetation dynamics induced by phreatophyte- water table interactions, J. Theor. Biol. 248 (2) (2007) 301–310.

[42] M. Gitterman, Bistable oscillator driven by two periodic fields, Journal of Physics A: Mathematical and General 34 (24) (2001) L355.

[43] I. I. Blekhman, P. S. Landa, Conjugate resonances and bifurcations in nonlinear systems under biharmonical excitation, Int. J. Nonlinear Mech. 39 (3) (2004) 421 – 426.

[44] S. Jeyakumari, V. Chinnathanmbi, S. Rajasekar, M. A. F. Sanjuan, Analysis of vibrational resonance in a quintic oscillator, Chaos 19 (043128) (2009) 1–8.

[45] S. Jeyakumari, V. Chinnathanmbi, S. Rajasekar, M. A. F. Sanjuan, Single and multiple vibrational resonance in a quintic oscillator with monostable potentials, Physics Review E 80 (046608) (2009) 1–8.

[46] S. Jeyakumari, V. Chinnathanmbi, S. Rajasekar, M. A. F. Sanjuan, Novel vibrational resonance in multistable systems, Int. J. of Bifurcation and Chaos 21 (1) (2011) 275–286.

[47] B. Deng, J. Wang, X. Wei, K. M. Tsang, W. L. Chan, Vibrational resonance in neuron populations, Chaos 20 (1) (2010) 013113.

[48] C. Jeevarathinam, S. Rajasekar, M. A. F. Sanjuán, Effect of multiple time-delay on vibrational resonance, Chaos 23 (1) (2013) 013136.

[49] H. Liu, X. Liu, J. Yang, M. Sanjuan, G. Cheng, Detecting the weak high-frequency character signal by vibrational resonance in the Duffing oscillator, Nonlinear Dyn. 89 (4) (2017) 2621–2628.

[50] S. Rajasekar, J. Used, A. Wagemakers, M. A. F. Sanjuan, Vibrational resonance in biological nonlinear maps, Commun. Nonlinear Sci. Numer. Simulat. 17 (2012) 3435–3445.

[51] S. Ghosh, D. Ray, Nonlinear vibrational resonance, Physics Review E 88 (042904) (2013) 1–8.

[52] C. Wang, K. Yang, Vibrational resonance in bistable gene transcriptional regulatory system, Chinese J. of Physics 50 (4) (2012) 606–617.

[53] J. Shi, C. Huang, T. Dong, X. Zhang, High-frequency and low-frequency effects on vibrational resonance in a synthetic gene network, Phys. Biol. 7 (3) (2010) 036006.

[54] S. Morfu, M. Bordet, On the correlation between phase-locking modes and vibrational resonance in a neuronal model, Commun. Nonlinear Sci. Numer. Simulat. 55 (2018) 277–286.
[55] T. Djomo Mbong, M. Siewe Siewe, C. Tchawoua, The effect of nonlinear damping on vibrational resonance and chaotic behavior of a beam fixed at its two ends and prestressed, Commun. Nonlinear Sci. Numer. Simulat. 22 (2015) 228–243.
[56] T. O. Roy-Layinde, J. A. Laoye, O. Popoola, U. E. Vincent, Analysis of vibrational resonance in bi-harmonically driven plasma, Chaos 26 (9) (2016) 093117.
[57] T. O. Roy-Layinde, J. A. Laoye, O. O. Popoola, U. E. Vincent, P. V. E. McClintock, Vibrational resonance in an inhomogeneous medium with periodic dissipation, Phys. Rev. E 96 (2017) 032209.
[58] U. E. Vincent, T. O. Roy-Layinde, O. O. Popoola, P. O. Adesina, P. V. E. McClintock, Vibrational resonance in an oscillator with an asymmetrical deformable potential, Phys. Rev. E 98 (2018) 062203.
[59] L. Ning, Z. Chen, Vibrational resonance analysis in a gene transcriptional regulatory system with two different forms of time-delays, Physica D 401 (2020) 132164.
[60] J. A. Laoye, T. O. Roy-Layinde, K. A. Omoteso, O. O. Popoola, U. E. Vincent, Vibrational resonance in a higher-order nonlinear damped oscillator with rough potential, Pramana 93 (6) (2019) 102.
[61] Z. Chen, L. Ning, Impact of depth and location of the wells on vibrational resonance in a triple-well system, Pramana J. Phys. 90 (4) (2018) 49.
[62] O. I. Olusola, O. P. Shomotun, U. E. Vincent, P. V. E. McClintock, Quantum vibrational resonance in a dual-frequency driven Tietz-Hua quantum well, Phys. Rev. E 101 (2020) 052216.
[63] P. Shibashis, R. Deb Shankar, Vibrational resonance in a driven two-level quantum system; linear and nonlinear response, Phil Trans Roy Soc. A 379 (2021) 20200231.
[64] T. O. Roy-Layinde, U. E. Vincent, S. A. Abolade, O. O. Popoola, J. A. Laoye, P. McClintock, Vibrational resonances in driven oscillators with position-dependent mass, Phil Trans Roy Soc. A 379 (2021) 20200227.
[65] Y. Ren, Y. Pan, F. Duan, Generalized energy detector for weak random signals via vibrational resonance, Physics Letters A 382 (12) (2018) 806 – 810.
[66] P. Jia, C. Wu, J. Yang, M. Sanjuan, G. Liu, Improving the weak aperiodic signal by three kinds of vibrational resonance, Nonlinear Dyn. 91 (4) (2018) 2699–2713.
[67] V. Chizhevsky, Amplification of an autodyne signal in a bistable vertical-cavity surface-emitting laser with the use of a vibrational resonance, Technical Physics Letters 44 (1) (2018) 17–19.
[68] J.-H. Yang, M. A. F. Sanjuán, H.-G. Liu, Enhancing the weak signal with arbitrary high-frequency by vibrational resonance in fractional-order Duffing oscillators, ASME J. Comput. Nonlinear Dyn 12 (5) (2017) 051011.
[69] J.-R. Yang, C.-J. Wu, J.-H. Yang, H.-G. Liu, On the weak signal amplification by twice sampling vibrational resonance method in fractional Duffing oscillators, ASME J. Comput. Nonlinear Dyn 13 (2018) 031009.
[70] Y. Ren, Y. Pan, F. Duan, F. Chapeau-Blondeau, D. Abbott, Exploiting vibrational resonance in weak-signal detection, Phys. Rev. E 96 (2017) 022141.
[71] T. Klinker, W. Meyer-Ilse, W. Lauterborn, Period doubling and chaotic behavior in a driven Toda oscillator, Physics Letters A 101 (8) (1984) 371–375.